The Journal of Immunology

Vibrio vulnificus VvpE Stimulates IL-1β Production by the Hypomethylation of the IL-1β Promoter and NF-κB Activation via Lipid Raft–Dependent ANXA2 Recruitment and Reactive Oxygen Species Signaling in Intestinal Epithelial Cells

Sei-Jung Lee, Young Hyun Jung, Eun Ju Song, Kyung Ku Jang, Sang Ho Choi and Ho Jae Han

J Immunol 2015; 195:2282-2293; Prepublished online 29 July 2015;
doi: 10.4049/jimmunol.1500951
http://www.jimmunol.org/content/195/5/2282

The Journal of Immunology is published twice each month by
The American Association of Immunologists, Inc.,
1451 Rockville Pike, Suite 650, Rockville, MD 20852

Print ISSN: 0022-1767 Online ISSN: 1550-6606.

Vibrio vulnificus VvpE Stimulates IL-1β Production by the Hypomethylation of the IL-1β Promoter and NF-κB Activation via Lipid Raft–Dependent ANXA2 Recruitment and Reactive Oxygen Species Signaling in Intestinal Epithelial Cells

Sei-Jung Lee,*,† Young Hyun Jung,*,† Eun Ju Song,*,† Kyung Ku Jang,‡ Sang Ho Choi,‡ and Ho Jae Han*,†

An inflammatory response is a hallmark of necrosis evoked by bacterial pathogens. *Vibrio vulnificus,* VvpE, is an elastase that is responsible for tissue necrosis and inflammation; however, the molecular mechanism by which it regulates host cell death has not been characterized. In the present study, we investigate the cellular mechanism of VvpE with regard to host cell death and the inflammatory response of human intestinal epithelial (INT-407) cells. The recombinant protein (r)VvpE (50 pg/ml) caused cytotoxicity mainly via necrosis coupled with IL-1β production. The necrotic cell death induced by rVvpE is highly susceptible to the knockdown of annexin A (ANXA)2 and the sequestration of membrane cholesterol. We found that rVvpE induces the recruitment of NADPH oxidase 2 and neutrophil cytosolic factor 1 into membrane lipid rafts coupled with ANXA2 to facilitate the production of reactive oxygen species (ROS). The bacterial signaling of rVvpE through ROS production is uniquely mediated by the phosphorylation of redox-sensitive transcription factor NF-κB. The silencing of NF-κB inhibited IL-1β production during necrosis. rVvpE induced hypomethylation and region-specific transcriptional occupancy by NF-κB in the IL-1β promoter and has the ability to induce pyroptosis via NOD-, LRR-, and pyrin domain–containing 3 inflammasome. In a mouse model of *V. vulnificus* infection, the mutation of the *vvpE* gene from *V. vulnificus* negated the proinflammatory responses and maintained the physiological levels of the proliferation and migration of enterocytes. These results demonstrate that VvpE induces the hypomethylation of the IL-1β promoter and the transcriptional regulation of NF-κB through lipid raft–dependent ANXA2 recruitment and ROS signaling to promote IL-1β production in intestinal epithelial cells. ***The Journal of Immunology*, 2015, 195: 2282–2293.**

The most prominent feature of host–pathogen interaction is the elicitation of a diverse array of host-protective and stress responses, such as cell death, proliferation, and inflammation (1). Specifically, the host cell death response caused as a consequence of a bacterial infection results in various modes of cell death, including apoptosis, necrosis, and pyroptosis. This process eventually disturbs the fine balance between host innate defense barriers, which may be a key element in the development of certain diseases (2). The anaerobic Gram-negative bacterium *Vibrio vulnificus* is a rod-shaped, curved, and motile pathogen with a single polar flagellum that causes serious and often fatal infections in humans. *V. vulnificus* infection is characterized by a high fatality rate of 70% in South Korea. It primarily affects people who are immunocompromised or have underlying diseases such as liver cirrhosis (3, 4). The most prominent aspect of *V. vulnificus* pathogenesis is its ability to infect a host via the gastrointestinal tract, after which it rapidly spreads from the small intestine to the blood stream (5). Although most of the virulence effects of *V. vulnificus* are known to derive from secreted toxins encoded by cytolytic pore-forming hemolysin (*VvhA*) (5) and multifunctional autoprocessing repeats in the toxin (*MARTXVv*) (5, 6), several other secreted and cell-associated factors of *V. vulnificus* have also been proposed as potential virulence determinants that are also involved in the pathogenesis of *V. vulnificus*. A 45-kDa elastase designated as *V. vulnificus* VvpE is considered to be another possible virulence factor of *V. vulnificus* (7, 8). Purified VvpE was proven to be lethal to mice and to induce hemorrhagic damage and dermonecrosis (8–10). Although previous research has raised some serious doubts about whether this enzyme is not a major virulence factor involved in mouse lethality (11), VvpE was shown to cause tissue necrosis and increased vascular permeability that are necessary for the invasion of this bacterium (7, 12). Additionally, VvpE has the ability to regulate the activity of host cell death–related enzymes (13) and is essential for bacterial swimming and survival to promote the virulence effect of *V. vulnificus* (14). To date, however, the underlying

*Department of Veterinary Physiology, College of Veterinary Medicine, Research Institute for Veterinary Science, Seoul National University, Seoul 151-741, South Korea; †Brain Korea 21 Program for Leading Universities and Students (BK21 PLUS) Creative Veterinary Research Center, Seoul National University, Seoul 151-741, South Korea; and ‡Department of Agricultural Biotechnology, National Research Laboratory of Molecular Microbiology and Toxicology, and Center for Food Safety and Toxicology, Seoul National University, Seoul 151-921, South Korea

Received for publication April 23, 2015. Accepted for publication June 25, 2015.

This work was supported by Grant 710002-07-5 from the Agriculture, Food and Rural Affairs Research Center Support Program, Ministry of Agriculture, Food and Rural Affairs, Republic of Korea (to H.J.H. and S.H.C.) and by Brain Korea 21 PLUS Program for Creative Veterinary Science Research.

Address correspondence and reprint requests to Prof. Ho Jae Han, Department of Veterinary Physiology, College of Veterinary Medicine, Seoul National University, Gwanak-ro, Gwanak-gu, Seoul 151-742, South Korea. E-mail address: hjhan@snu.ac.kr

Abbreviations used in this article: ANXA, annexin A; 5-Aza, 5-azacytidine; ChIP, chromatin immunoprecipitation; CM-H_2DCFDA, 2′,7′-dichlorofluorescein diacetate; CTB, cholera toxin subunit B; i.g., intragastric(ally); LB, Luria–Bertani; MβCD, methyl-β-cyclodextrin; MOI, multiplicity of infection; MSP, methyl-specific PCR; NAC, *N*-acetyl-L-cysteine; NCF1, neutrophil cytosolic factor 1; NLRP3, NOD-, LRR-, and pyrin domain–containing 3; NOX, NADPH oxidase; PI, propidium iodide; qRT-PCR, quantitative real-time PCR; ROS, reactive oxygen species; rVvpE, recombinant protein VvpE; siRNA, small interfering RNA; WT, wild-type.

cellular mechanisms of VvpE with regard to host cell death and the inflammatory response involved in this process remain largely unknown.

Whereas necrosis is associated with caspase-independent inflammation accompanied by nuclear swelling and the release of cellular contents, pyroptosis has been characterized as a programmed cell death coordinated by inflammasome-mediated caspase-1 activation that results in maturation of the proinflammatory cytokines IL-1β and IL-18 (2, 15). Pyroptosis is crucial for controlling microbial infections and can be regulated by reactive oxygen species (ROS) production, potassium efflux, or lysosomal damage (2, 15, 16). Epigenetic control of gene expression during a pathogenic bacterial infection is another important element in the regulation of host cell death. A recent report showed that many enteric bacterial pathogens, such as *Salmonella typhimurium* (17, 18), *Helicobacter pylori* (19), and the enteropathogenic *Escherichia coli* (EPEC) (20), affect a diverse set of epigenetic factors such as DNA methylation and histone modification to regulate the selective activation or silencing of specific host genes (21). Thus, studies regarding the process leading to pathogen-induced cell death are likely to be critical to uncovering the mechanisms of pathogenesis. However, there are no previous reports related to the molecular mechanisms of VvpE action, which drive the transcriptional and epigenetic regulation of the inflammatory process during the necrosis of intestinal epithelial cells. In this study, therefore, we investigate the VvpE signaling pathway that leads to host cell death coupled with the inflammatory response and evaluate the functional importance of VvpE in a mouse model of *V. vulnificus* infection.

Materials and Methods

Chemicals

FBS was purchased from BioWhittaker (Walkersville, MD). The following Abs were purchased: NADPH oxidase (NOX)2, annexin A (ANXA)2, and ANXA4 Ab (BD Biosciences, Franklin Lakes, NJ); neutrophil cytosolic factor 1 (NCF1) Ab (LifeSpan Biosciences, Seattle, WA); p–NF-κBp65, NF-κBp65, IL-1βp17, caspase-1p10, and β-actin Abs (Santa Cruz Biotechnology, Paso Robles, CA); HRP-conjugated goat anti-rabbit and goat anti-mouse IgG Abs (Jackson ImmunoResearch Laboratories, West Grove, PA). 2′,7′-Dichlorofluorescein diacetate (CM-H_2DCFDA) was obtained from Invitrogen (Carlsbad, CA). Methyl-β-cyclodextrin (MβCD), *N*-acetyl-L-cysteine (NAC), and 5-azacytidine (5-Aza) were purchased from Sigma-Aldrich (St. Louis, MO). The concentrations of all of the pharmacological inhibitors listed did not show any significant cytotoxic effects by themselves as confirmed by FACS analysis in each experiment. All other reagents were of the highest purity commercially available and were used as received.

Cells

Human intestinal epithelial (INT-407) and RAW 264.7 murine macrophage cells were purchased from American Type Culture Collection (Manassas, VA). INT-407 cells were grown at 37˚C in 5% CO_2 in α-MEM supplemented with 10% FBS and antibiotics (10 U/ml penicillin G and 10 μg/ml streptomycin). INT-407 cells have previously been used to evaluate the function of virulence factors of *V. vulnificus* in regulation of proinflammatory process (22), cytotoxic effect (23), and cell adherence ability (24). Alternatively, RAW 264.7 cells were cultured at 37˚C in 5% CO_2 in RPMI 1640 containing 10% FBS and antibiotics.

Overexpression and purification of the recombinant elastolytic protease VvpE

To find the functional role of VvpE in INT-407 cells, we have previously prepared a recombinant protein of VvpE (rVvpE). Briefly, the coding region of *vvpE* encoding an elastolytic protease was amplified and then subcloned into a His_6 tag expression vector, pET29a(+) (Novagen, Madison, WI), resulting in pKS1202 (25). *E. coli* BL21 (DE3) harboring the pKS1202 was grown in Luria–Bertani (LB)/ampicillin media at 37˚C until the cultures reached an A_{600} between 0.5 and 0.6. The temperature was lowered to 30˚C, and protein expression was induced by treatment with 1 mM isopropyl β-D-thiogalactoside for 6 h. The cells were harvested by centrifugation at 5000 × *g* for 20 min at 4˚C. The cell pellets were resuspended in buffer A (20 mM Tris-Cl [pH 8.0], 500 mM NaCl), and the cell suspensions were ultrasonicated. The crude cell extracts were centrifuged at 16,000 × *g* for 30 min at 4˚C and the supernatant was filtrated using a 0.2-μm Whatman Puradisc syringe filter (Whatman International, Maidstone, U.K.) for isolating the soluble fraction. Cell lysate containing His_6-tagged VvpE protein was mixed with 1 ml Ni-NTA agarose (Qiagen, Valencia, CA) for 1 h at 4˚C and the mixture was loaded on Bio-Spin chromatography columns (Bio-Rad Laboratories, Herculus, CA). The resin was washed with buffer A, and bound VvpE protein was eluted with buffer A containing 300 mM imidazole. After purification, the homogeneity of VvpE was assessed by 12% SDS-PAGE and Coomassie blue staining. Purified proteins was dialyzed against 20 mM Tris-Cl [pH 8.0] concentrated to 0.3 mg/ml using Slide-A-Lyzer dialysis cassettes (Thermo Scientific, Hudson, NH) and stored at −80˚C until use. We have further checked the LPS contamination in rVvpE protein by using an endotoxin quantitation kit (Pierce LAL chromogenic endotoxin quantitation kit, Thermo Fisher Scientific, Waltham, MA). The level of endotoxin in 50 pg/ml rVvpE was <0.004 endotoxin units. Thus, we suggest that rVvpE is a purified recombinant protein containing a very low level of endotoxin and suitable for our experiments in this study.

MTT cell viability assay

Cell viability was determined using the conversion of MTT to formazan via mitochondrial oxidation. Cells were pretreated with indicated inhibitors prior to rVvpE exposure for various times. MTT solution was then added to each well at a final concentration of 1 mg/ml per well and the plates were incubated at 37˚C for another 2 h. After incubation, 150 μl DMSO was added to each well to dissolve the formazan formed and the absorbance was read at 570 nm using a spectrophotometer.

[^{3}H]thymidine incorporation

The [^{3}H]thymidine incorporation experiments were performed as previously described by Brett et al. (26). Briefly, cells were synchronized by serum starvation for 24 h and then exposed to 50 pg/ml rVvpE for 24 h. After the incubation period, 1 μCi [methyl-^{3}H]thymidine (sp. act., 74 GBq/mmol, 2.0 Ci/mmol; Amersham Biosciences, Buckinghamshire, U.K.) was added to the cultures for 1 h at 37˚C. Cellular [^{3}H]thymidine uptake was quantified by liquid scintillation counting of harvested cellular material (Wallac, Turku, Finland). All values were converted from absolute counts to percentages of control.

Flow cytometry

INT-407 cells were synchronized in the G_0/G_1 phase by culture in serum-free media for 24 h before incubation of rVvpE. The necrotic cell death was detected with an Annexin V and propidium iodide (PI) staining kit (BD Biosciences) according to the manufacturer's instructions. Briefly, the cells were detached with 0.05% trypsin/EDTA and 1 × 10^5 cells were resuspended with annexin V binding buffer. The cells were then stained with annexin V (25 μg/ml) and PI (125 ng/ml) and incubated for 15 min at room temperature in the dark. The sample was read by flow cytometry and analyzed using CXP software (Beckman Coulter, Brea, CA). Samples were gated to exclude debris (forward light scatter [FSC] area versus side scatter area), and then any cell doublets were excluded using FSC area versus FSC width analysis.

Apoptosis/necrosis detection

Cell death was also detected with an apoptosis/necrosis detection kit (Abcam, Cambridge, MA) according to the manufacturer's instructions. Briefly, the cells were treated with Apopxin green indicator as a phosphatidylserine marker and 7-aminoactinomycin D and were then incubated in the dark for 60 min at room temperature. After the cells were rinsed with ice-cold PBS, the level of cell death was examined using a luminometer (Victor3; PerkinElmer, Waltham, MA) and quantified by measuring absorbance at excitation and emission wavelengths of 490 and 525 nm for detection of Apopxin green indicator or at excitation and emission wavelengths of 490 and 650 nm for detection of 7-aminoactinomycin D.

Small interfering RNA transfection

Cells were grown until 75% of the surface of the plate and transfected for 36 h with ON-TARGETplus small interfering RNAs (siRNAs) mixed by four different siRNAs specific for *ANXA2*, *ANXA4*, or *NF-κβp65* (GE Dharmacon, Lafayette, CO) or nontargeting siRNA as a negative control (GE Dharmacon) with HiPerFect transfection reagent (Qiagen, Valencia,

CA) according to the manufacturers' instructions. The siRNA efficacy for ANXA2, ANXA4, caspase-1, NOD-, LRR-, and pyrin domain–containing 3 (NLRP3), and NF-κBp65 determined by Western blotting was 59, 62, 70, 72, and 67%, respectively.

RNA isolation and RT-PCR

Total RNA was extracted using the RNeasy Plus mini kit (Qiagen). Reverse transcription was carried out with 3 μg RNA using a Maxime RT premix kit (iNtRON Biotechnology, Sungnam, Korea). β-Actin was used as an endogenous control. The cDNA (5 μl) for the annexins family was amplified.

Quantitative real-time PCR

The real-time quantifications of proinflammatory cytokines were performed using a Rotor-Gene 6000 real-time thermal cycling system (Corbett Research, Mortlake, NSW, Australia) with a QuantiMix SYBR Kit (PhileKorea Technology, Daejeon, Korea) according to the manufacturers' instructions. β-Actin was used as an endogenous control.

IL-1β ELISA

INT-407 and RAW 264.7 cells plated on 60-mm culture dishes were grown in FBS-free medium for 24 h and divided into groups according to the experimental protocol. The IL-1β concentration in the culture medium was quantified by an ELISA (R&D Systems, Minneapolis, MN) according to the manufacturer's instructions.

Immunoprecipitation and Western blot analysis

Interaction of ANXA2 with NOX2, NCF1, or caveolin-1 was analyzed by immunoprecipitation and Western blotting. Cells were lysed with lysis buffer (1% Triton X-100 in 50 mM Tris-HCl [pH 7.4] containing 150 mM NaCl, 5 mM EDTA, 2 mM Na_3VO_4, 2.5 mm Na_4PO_7, 100 mm NaF, 200 nm microcystin lysine–arginine, and protease inhibitors). Cell lysates (400 μg) were mixed with 10 μg of each Ab. The samples were incubated for 4 h, mixed with protein A/G Plus–agarose immunoprecipitation reagent (Pierce, Rockford, IL) and then incubated for an additional 12 h. The beads were washed four times and the bound proteins were released from the beads by boiling in SDS-PAGE sample buffer for 5 min. Samples were analyzed by Western blotting, which was performed as previously described with minor modifications (27).

Detergent-free purification of caveolin-rich membrane fraction

INT-407 cells were washed twice with ice-cold PBS, scraped into 2 ml 500 mM sodium carbonate (pH 11.0), transferred to a plastic tube, and homogenized with a Sonicator 250 apparatus (Branson Ultrasonic, Danbury, CT) using three 20-s bursts. The homogenate was adjusted to 45% sucrose by the addition of 2 ml 90% sucrose prepared in MES-buffered solution consisting of 25 mM MES buffer solution (pH 6.5) and 0.15 M NaCl and placed at the bottom of an ultracentrifuge tube. A 5–35% discontinuous sucrose gradient was formed (4 ml each of 5 and 35% sucrose, both in MES buffer solution containing 250 mM sodium carbonate) and centrifuged at 40,000 × *g* for 20 h in a Beckman SW41 Rotor (Beckman Coulter, Fullerton, CA). Twelve fractions were collected and analyzed by 12% SDS-PAGE.

Intracellular reactive oxygen species detection

CM-H_2DCFDA was used to detect the general reactive oxygen species (ROS) production. To quantify the intracellular ROS levels, the cells treated with 10 mM DCF-DA were rinsed twice with ice-cold PBS and then scraped. A 100-μl cell suspension was loaded into a 96-well plate and examined using a luminometer (Victor3; PerkinElmer) and a fluorescent plate reader at excitation and emission wavelengths of 485 and 535 nm, respectively.

Immunofluorescence analysis

Either INT-407 cells or ileum frozen sections were fixed in 4% paraformaldehyde in PBS for 10 min at room temperature, permeabilized in 0.1% Triton X-100 in PBS for 5 min, and blocked in PBS containing 5% (v/v) normal goat serum for 30 min at room temperature. Samples were then stained with primary Ab for overnight at 4°C. Following three washes with PBS, the samples were incubated with Alexa Fluor 488–conjugated goat anti-rabbit/mouse IgM (Invitrogen, Carlsbad, CA, USA) and counterstained with PI in PBS containing 5% (v/v) normal goat serum for 2 h. After washing with PBS, samples were mounted on slides and visualized with an Olympus FluoView 300 confocal microscope with a ×400 objective.

Chromatin immunoprecipitation

Chromatin immunoprecipitation (ChIP) was performed using the EZ-ChIP kit (EMD Millipore, Billerica, MA) according to the manufacturer's protocol. Briefly, cells were treated with 1% formaldehyde for 15 min to cross-link proteins to DNA, lysed, and then sonicated. The lysate was incubated with primary Abs overnight at 4°C. The immunocomplex was purified by incubation with 60 μl protein G–agarose beads for 1 h and eluted for DNA purification. Quantitative real-time PCR (qRT-PCR) was performed with primers for the *IL-1β* promoter flanking the putative NF-κBp65 binding sites. The following primer sequences of *IL-1β* promoter were used (sense and antisense, respectively): −488 to −327 bp, 5′-GGTAGAGACCCACACCCTCA-3′ and 5′-TGGGACAAAGTGGAAGACAC-3′; −347 to −174bp, 5′-GTGTCTTCCACTTTGT CCCA-3′ and 5′-CATGGAAGGGCAAGGAGTAG-3′. Anti-RNA polymerase II and normal mouse IgG were used as the positive and negative control for immunoprecipitation, respectively. The human *IL-1β* promoter sequence was found using the Eukaryotic Promoter Database. The putative binding sites were predicted using Alggen Promo software, version 3.0.2 (28, 29).

Methylation analysis

Genomic DNA from INT-407 cells was prepared with the QIAamp DNA mini kit (Qiagen). The extracted DNA was treated with sodium bisulfite using an EzWay DNA methylation detection kit according to the manufacturer's instructions (Koma Biotech, Seoul, Korea). The methylation status of *IL-1β* gene in INT-407 cells was determined by methyl-specific PCR (MSP) analysis. We conducted MSP of *IL-1β* gene promoter at −299 CpG sites. The following primer sequences for the −299 CpG sites of *IL-1β* promoter were used (sense and antisense, respectively): methylated, 5′- ATATATTAAATTTAAATATTTTTTTAACGT-3′ and 5′-TACAAATATACATTATTTTCCTAACAATCG-3′; unmethylated, 5′-TATATATTAAATTTAAATATTTTTTTAATG-3′ and 5′-ACAAATATACATTATTTTCCTAACAATCAT-3′.

Bacterial strains, plasmids, and culture media

The strains and plasmids used in this study are listed in Table I. All *V. vulnificus* strains (M06-24/O and M06-24/O *vvpE*) are isogenic and naturally resistant to polymyxin B. Unless otherwise noted, *V. vulnificus* strains were grown in LB medium supplemented with 2.0% (w/v) NaCl (LBS) at 30°C. All media components were purchased from Difco Laboratories (Detroit, MI). *V. vulnificus* was grown to midlog phase (A_{600} of 0.500) corresponding to 2×10^8 CFU/ml and centrifuged at 6000 × g for 5 min. The pellet was washed with PBS and adjusted to desired CFU/ml based on the A_{600} determined using an UV–visible spectrophotometer (UV-1800, Shimadzu, Kyoto, Japan) to estimate culture density.

Mouse model and colonization assay

All animal procedures were performed following the National Institutes of Health guidelines for the humane treatment of animals, with approval from the Institutional Animal Care and Use Committee of Seoul National University (SNU-140108-4). Seven-week-old mice ($n = 10$) were received intragastric (i.g.) inoculation of boiled *V. vulnificus* (control), *V. vulnificus* (wild-type [WT]), and a mutant deficient in *vvpE* gene in *V. vulnificus* (M06-24/O *vvpE, vvpE* mutant) at 1.1×10^6 CFU/ml for 18 h and sacrificed. Mice ileum tissue was collected, washed, and homogenized. The homogenates of each organ were serially diluted and spread on LB agar containing polymyxin B (100 U/ml). CFUs were normalized to grams of intestinal tissues (CFU/g) to represent superficial bacterial counts. Note that the mice were given BrdU (50 mg/kg) by i.p. injections for 2 or 48 h prior to the sacrifice. Half of ileum tissues were removed, flushed with ice-cold PBS, and stored at −70°C for protein and RNA analysis. The other half were embedded in OCT compound and stored at −70°C. Samples were then cut into 6-μm-thick frozen sections.

Wound-healing migration assay

INT-407 cells were seeded at 4×10^4 cells on low 35-mm dishes with both silicone reservoirs, which are separated by a 500-μm-thick wall (Ibidi, Martinsried, Germany) (30) and incubated until the cell reached ~100% confluence in serum containing medium. After serum starvation, the silicone reservoirs were removed with sterile forceps to create a wound field. The cells were incubated for an additional 6 h with rVvpE (50 pg/ml) in the presence of 1% FBS and visualized with an Olympus FluoView 300 confocal microscope with a ×100 objective.

Oris cell migration assay

INT-407 cells were seeded at 3×10^2 cells/100 μl in an Oris well (Platypus Technologies, Madison, WI) and incubated for 24 h to permit cell

Table I. Plasmids and bacterial strains used in this study

Strain or Plasmid	Relevant Characteristics	Reference or Source
Bacterial strains		
V. vulnificus		
M06-24/O	Clinical isolate; virulent; WT	Laboratory collection
CMM111	MO6-24/O *vvpE*::pKC9844; elastase deficient; *ΔvvpE*	Jeong et al. 2000 (11)
E. coli		
BL21 (DE3)	F^- *ompT hsdS*$_B$ ($r_B^- m_B^-$) *gal dcm* (DE3)	Laboratory collection
DH5α	λ^- ϕ80d*lacZ*ΔM15 Δ(*lacZYA-argF*)*U169 recA1 endA1 hsdR17* ($r_K^- m_K^-$) *supE44 thi-1 gyrA relA1*; plasmid replication	Laboratory collection
S17-1λ*pir*	λ-*pir* lysogen; *thi pro hsdR hsdM*$^+$ *recA* RP4-2 Tc::μ-Km::Tn7;Tp^r Sm^r; host for π-requiring plasmids; conjugal donor	Laboratory collection
Plasmids		
pET29a(+)	His_6 tag fusion expression vector; Kn^r	Novagen
pKS1202	pET29a(+) with 1,827-bp *vvpE*; Kn^r	Kim et al. 2013 (25)
pVSV102	$OriV_{R6K\gamma}$ $oriT_{RP4}$ $oriV_{pES213}$ Kn^r *gfp*	Dunn et al. 2013 (53)

Kn^r, kanamycin resistant; Sm^r, streptomycin resistant; Tp^r, trimethoprim resistant.

adhesion. When the cell reached ~70% confluence, cells were then incubated with serum-free medium and the inserts were carefully removed. The cells were incubated for an additional 6 h with rVvpE (50 pg/ml) in the presence of 1% FBS and visualized with an Olympus FluoView 300 confocal microscope with a ×100 objective. Cell populations in endpoint assays were stained with 5 μM calcein AM for 30 min. Migrated cells were quantified through measurement of fluorescence signals by using a microplate reader at excitation and emission wavelengths of 485 and 515 nm, respectively (31).

Host cell infection protocol

INT-407 and RAW 264.7 cells (1×10^6 cells/ml) grown to confluence in six-well plates were incubated in serum/antibiotic-free media for 24 h. The bacterial suspensions in serum/antibiotic-free media were added to the cells at a multiplicity of infection (MOI, ratio of number of bacteria to number of epithelial cells) of 1, 5, and 10, after which the infected cells were incubated for 1 h. For IL-1β ELISA, coculture supernatants were obtained and harvested by centrifugation at 4000 × *g* for 10 min at 4°C. This was repeated once more with the resulting supernatant. The clarified supernatants were filtered through a 0.22-μm pore membrane to ensure the removal of any remaining bacterial cells and debris. For *IL-1β* qRT-PCR, total RNA was extracted from the INT-407 and RAW 264.7 cells.

Statistical analysis

Results are expressed as mean ± SEM. All experiments were analyzed by ANOVA, followed in some cases by a comparison of treatment means with a control using the Bonferroni–Dunn test. Differences were considered statistically significant at $p < 0.05$.

Results

VvpE induces proinflammatory response during the necrosis of intestinal epithelial cells

To find the functional role of VvpE, human intestinal epithelial (INT-407) cells were exposed to various concentrations (0–200 pg/ml) of rVvpE for 6 h. rVvpE significantly induced cytotoxicity of INT-407 cells from 50 to 200 pg/ml, compared with the cells with no treatment (Fig. 1A). An increase in cytotoxicity was observed after 6 h of incubation with 50 pg/ml rVvpE (Fig. 1B). The results after the [^{3}H]thymidine incorporation of INT-407 cells also revealed that 50 pg/ml rVvpE significantly attenuated the level of DNA synthesis, compared with the vehicle (Fig. 1C). We further performed flow cytometric analyses using PI and annexin V for identification of necrotic and apoptotic cells caused by rVvpE treatment (Fig. 1D). rVvpE significantly induced the necrotic cell death (a 5.1 ± 0.3-fold increase compared with the vehicle) of INT-407 cells, whereas for apoptotic cell death, this shows a marginal effect (a 1.9 ± 0.3-fold increase compared with the vehicle). We further confirmed the necrosis-promoting effect of rVvpE by using another reagent that monitors the apoptotic cells with annexin V as well as the necrotic cells with 7-aminoactinomycin D, a fluorescent membrane-impermeable red dye, which has strong affinity GC-rich regions of DNA. As shown in Fig. 1E, we found that rVvpE has relatively more stimulatory potency on the necrotic cell death than on the apoptotic cell death, confirming that rVvpE is essential for triggering the necrotic cell death rather than the apoptosis. This result suggests that the functional role of rVvpE to induce cell death is reproducible in different assays. We further assessed whether rVvpE evokes proinflammatory response, which is typically caused by necrotic cell death. rVvpE increased the expression of proinflammatory cytokines, including IL-1β, IL-6, and TNF-α from 6 h in INT-407 cells (Fig. 1F). Among the proinflammatory cytokines, the induction of IL-1β was particularly susceptible to the rVvpE treatment and its mRNA expression was significantly upregulated from 2 h after incubation with 50 pg/ml rVvpE (Fig. 1G). We also explored the ability of rVvpE to regulate IL-1β production in an ELISA assay. In contrast to the control, 50 pg/ml rVvpE evoked a substantial induction of IL-1β secretion from 6 h (Fig. 1H). These data provide the important evidence that rVvpE regulates the expression and secretion of IL-1β during necrotic cell death in intestinal epithelial cells. To ensure the role of VvpE in IL-1β activation, INT-407 cells were exposed to various MOI (ratio of number of bacteria to number of host cells) of *V. vulnificus* (WT) and a mutant deficient in *vvpE* gene in *V. vulnificus* (*VvpE* mutant). An increase in the expression and production of IL-1β was observed at 1 h after incubation with 10 MOI of WT, whereas *VvpE* mutant negated the IL-1β activation (Fig. 1I). More than 80% of the detached cells and the cell destruction were exhibited from 2 h after incubation with 10 MOI of WT (data not shown). The *VvpE* mutant at 10 MOI also has the ability to prevent the activation of IL-1β induced by WT in RAW 264.7 murine macrophage cells (Fig. 1J). This result suggests that VvpE plays a critical role in IL-1β activation and the functional role of VvpE to induce IL-1β activation is reproducible with other types of immune cells.

ANXA2 is required for the necrosis and inflammation induced by VvpE

Annexin As (ANXAs) are thought to confer diverse cellular processes such as cell growth and inflammation as multifunctional proteins. The expression of ANXAs on the cell surface is thought to serve as a receptor that regulates several membrane-related events, such as exo/endocytosis (32) and membrane–cytoskeletal interaction (33). We first determined the existence of ANXA isotypes in INT-407 cells. ANXAs are expressed in the order of *ANXA1*, *ANXA2*, *ANXA4*, *ANXA5*, *ANXA6* > *ANXA8*, *ANXA9*, *ANXA10*, *ANXA11* > *ANXA7* (Fig. 2A). The expression of *ANXA3* and

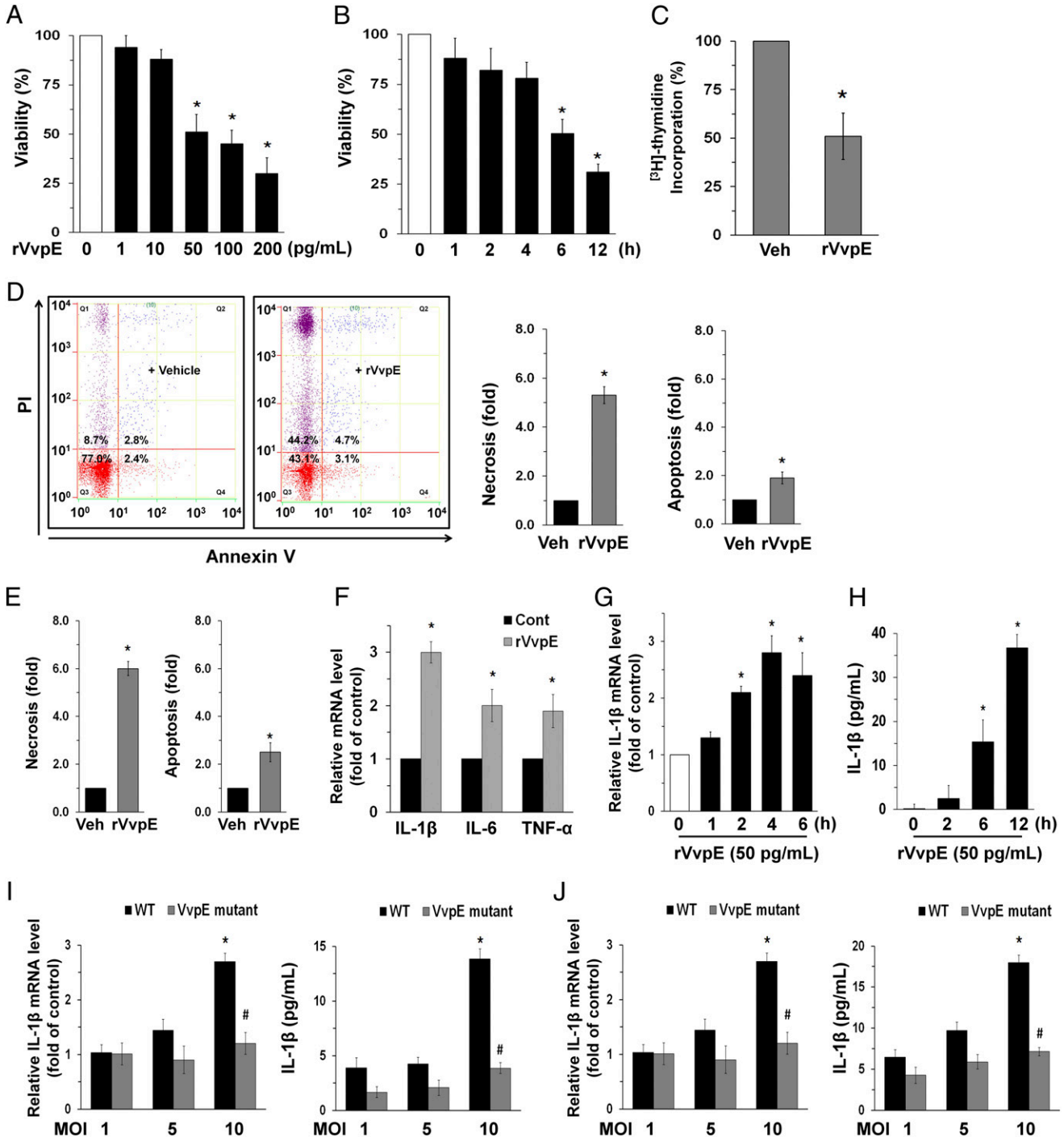

FIGURE 1. VvpE induces proinflammatory response during the necrosis of intestinal epithelial cells. (**A**) Dose responses of rVvpE for 6 h in MTT assay are shown. (**B**) Time responses of 50 pg/ml rVvpE in MTT assay are shown. (**C**) [^{3}H]thymidine incorporation was determined by treatment with 50 pg/ml rVvpE for 6 h in INT-407 cells. (**D**) Cells were incubated with rVvpE for 6 h. Percentages of necrosis, survival, and apoptosis were measured by using PI/annexin V staining and flow cytometry (*left panel*). PI/annexin V cells (Q1) were considered necrotic, PI/annexin V double-positive cells (Q2) were considered late apoptotic, PI/annexin V cells (Q3) were considered alive, and PI/annexin V cells (Q4) were considered early apoptotic. Quantitative analysis of the fold changes of necrotic (Q1) and apoptotic (Q2+Q4) cells by FACS analysis is shown (right panel). (**E**) Quantitative analysis of the fold changes of apoptotic and necrotic cells by an apoptosis/necrosis detection kit is shown. (**F**) Expression of proinflammatory cytokines is shown. Time responses of rVvpE in *IL-1β* expression and IL-1β secretion were evaluated by qRT-PCR (**G**) and ELISA (**H**), respectively. *IL-1β* expression and IL-1β secretion in INT-407 (**I**) and RAW 264.7 cells (**J**) infected with of WT and *VvpE* mutant at 1, 5, and 10 MOI for 1 h are shown. (A–H) Data represent mean ± SEM. $n = 5$. $^*p < 0.05$ versus control or vehicle (Veh, boiled rVvpE, 50 pg/ml). (I and J) Data represent mean ± SEM $n = 5$. $^*p < 0.05$ versus control. $^\#p < 0.01$ versus 10 MOI of WT.

ANXA13 were not detected in these cell lines. Because it was previously shown that ANXA2 and ANXA4 of all the ANXA isoforms are essential in pathogenesis of bacterial infection (34, 35), we then determined the involvement of ANXA2 and ANXA4 in the necrotic cells death elicited by rVvpE (Fig. 2B). Interestingly, the cytotoxic effect of rVvpE was significantly silenced by the knockdown of ANXA2. Knockdown of ANXA4 by siRNA did not show any significant effect on necrotic cell death in rVvpE-treated INT-407 cells. Additionally, IL-1β production by rVvpE was markedly inhibited by knockdown of ANXA2, not by

ANXA4 (Fig. 2C). These results suggest that ANXA2 is critically involved in proinflammatory response during the necrosis. Cholesterol in plasma membrane has been thought to be one of the cellular receptors of *V. vulnificus* (36). To confirm the structural importance of membrane rafts in the rVvpE-mediated signaling pathway, we employed the lipid raft sequester MβCD, which is known to deplete cholesterol from the cell membrane. Interestingly, MβCD significantly attenuated the necrotic cell death (a 2.7 ± 0.5-fold decrease compared with the rVvpE alone) (Fig. 2D) as well as the production of IL-1β in INT-407 cells (Fig. 2E), suggesting that rVvpE in acting through lipid raft is essential for triggering the proinflammatory signaling pathway during the necrotic cell death. We then determined how rVvpE links to the activation of ANXA2 within lipid raft by means of discontinuous sucrose density-gradient centrifugation. Fig. 2F shows that the lipid raft markers caveolin-1 and flotillin-2 were found in mainly fraction 6. ANXA2 was highly enriched in fractions 9–12 representing non–lipid raft parts of membrane. Interestingly, an increase in the level of ANXA2 appeared in fractions 5 and 6 after incubation with 50 pg/ml rVvpE compared with the vehicle alone, suggesting that rVvpE enhances the recruitment of ANXA2 into lipid rafts. Moreover, the subunits of NOX enzymes, NOX2 ($gp91^{phox}$) and NCF1 ($p47^{phox}$), were highly enriched in fractions 10–12. However, rVvpE treatment resulted in translocations of NOX2 and NCF1 into fraction 6, including lipid rafts part. The effect of rVvpE on the membrane location of ANXA2 was further visualized by staining the ANXA2 and lipid raft marker molecule, cholera toxin subunit B (CTB). As shown in Fig. 2G, rVvpE significantly increased the colocalization of CTB with ANXA2. Because the above approaches are qualitative at best, we further tried to quantify the results by using coimmunoprecipitation of ANXA2 with proteins related to the lipid rafts in the presence of

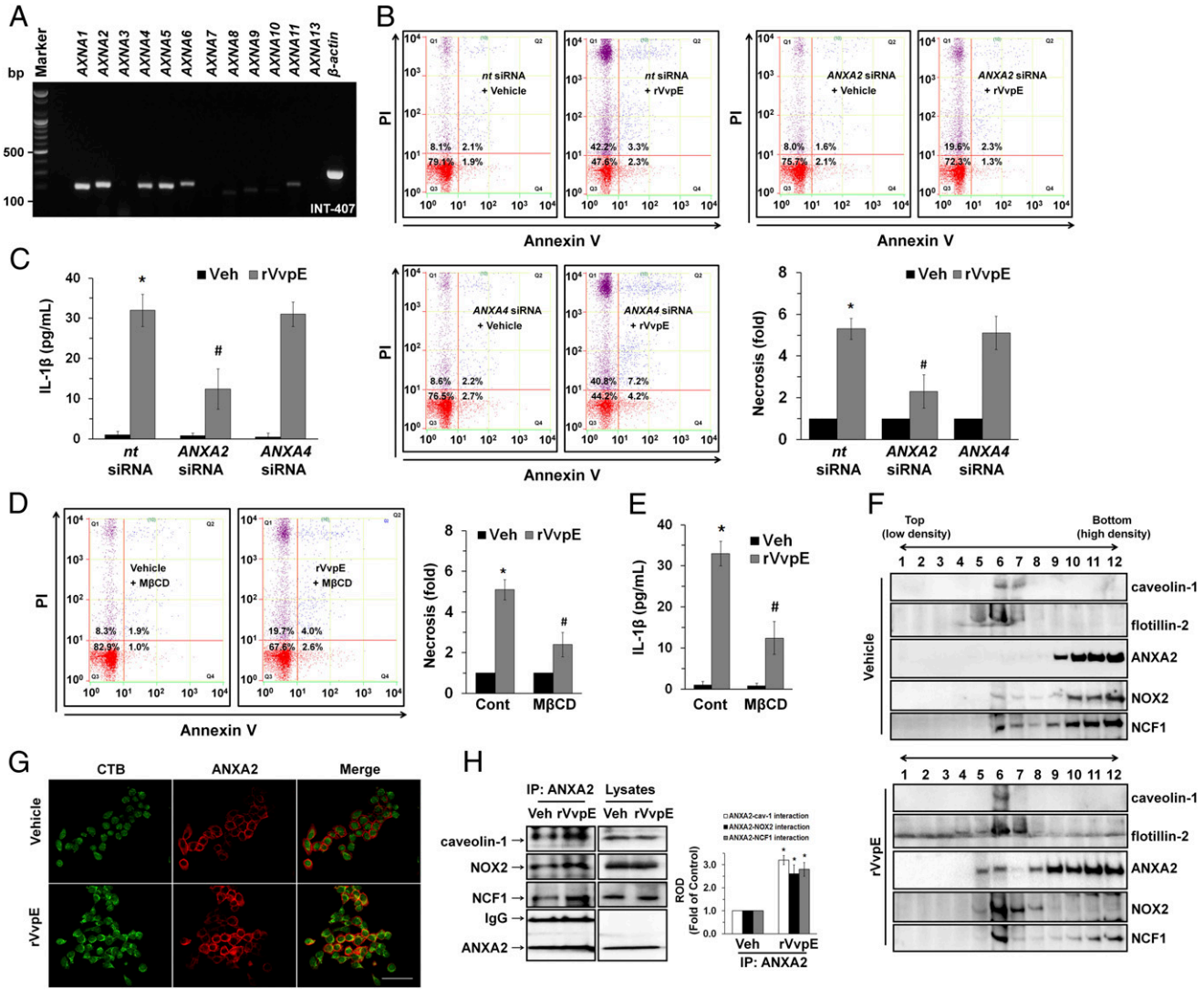

FIGURE 2. ANXA2 is required for the necrosis and inflammation induced by VvpE. (**A**) Expression of *ANXA* mRNAs in INT-407 cells is shown. $n = 5$. Cells transfected with siRNAs for nontargeting (nt) control, ANXA2, and ANXA4 were incubated with rVvpE for 6 h. (**B**) FACS analysis and quantitative analysis of the percentage of necrotic (Q1) cells are shown. $n = 4$. (**C**) The level of IL-1β protein was quantified by ELISA. $n = 5$. Cells were pretreated with MβCD (0.1 mM) for 1 h prior to rVvpE exposure for 6 h. (**D**) FACS analysis and quantitative analysis of the percentage of necrotic (Q1) cells are shown. $n = 4$. (**E**) The level of IL-1β protein was quantified by ELISA. $n = 5$. INT-407 cells were incubated in the presence of rVvpE (50 pg/ml) for 30 min. (**F**) Caveolin-enriched membrane fractions were prepared by discontinuous sucrose density gradient fractionation, and the location of caveolin-1, flotillin-2, ANXA2, NOX2, and NCF1 was determined by Western blot analysis. $n = 3$. (**G**) The increased colocalization of CTB (green) with ANXA2 (red) was determined by confocal microscopy using immunofluorescence staining. Scale bars, 100 μm (original magnification ×400). $n = 3$. (**H**) ANXA2 coimmunoprecipitated with caveolin-1, NOX2, and NCF1 (*left*). Expression of caveolin-1, NOX2, NCF1, and ANXA2 in total cell lysates is shown (*right*). (B–E and H) Data represent mean ± SEM. $^{*}p < 0.01$ versus nontargeting siRNA plus vehicle (Veh) or Veh alone. $^{\#}p < 0.05$ versus rVvpE.

rVvpE. It was noted that ANXA2 coimmunoprecipitated with caveolin-1, NOX2, and NCF1, and, importantly, that these interactions were enhanced by the rVvpE treatment (Fig. 2H). This means that lipid raft–mediated clustering of ANXA2, NOX2, and NCF1 is required to trigger the bacterial signaling pathway induced by rVvpE in INT-407 cells.

Regulatory effect of VvpE on ROS production and NF-κB phosphorylation

Clustering of NOX enzymes facilitates the production of ROS, which results in a prominent amplification of the transmembrane signal (37). A significant increase in the ROS level appeared after incubation with 10–50 pg/ml for 30 min compared with the vehicle alone (Fig. 3A, *left panel*). The increase in ROS production was transiently augmented between 0.5 and 1 h after incubation with 50 pg/ml rVvpE (Fig. 3A, *right panel*). Additionally, a pretreatment with MβCD as well as silencing of *ANXA2* significantly blocked rVvpE-induced ROS production (Fig. 3B). Antioxidant NAC was used as a positive control. The inhibitory effects of MβCD and *ANXA2* siRNA on ROS production were further visualized by staining INT-407 cells with a fluorescent dye, CM-H_2DCFDA (Fig. 3C). Consistently, pretreatment with the NAC significantly blocked the necrotic cell death (Fig. 3D) as well as the production of IL-1β in INT-407 cells (Fig. 3E). These data suggest an involvement of ROS production in promoting necrotic cell death and proinflammatory response induced by rVvpE. We further examined the role of rVvpE in activation of NF-κB, which is a direct transcriptional target for necrotic signaling pathway as well as inflammation. As shown in Fig. 3F, NF-κBp65 phosphorylation increased between 1 and 3 h after incubation with 50 pg/ml rVvpE. The increased accumulation of NF-κBp65 phosphorylation in the nucleus was further confirmed by immunofluorescence staining and counterlabeling with PI (Fig. 3F, *right panel*). Additionally, the phosphorylation of NF-κBp65 evoked by a treatment with rVvpE was markedly inhibited by pretreatment with the MβCD and

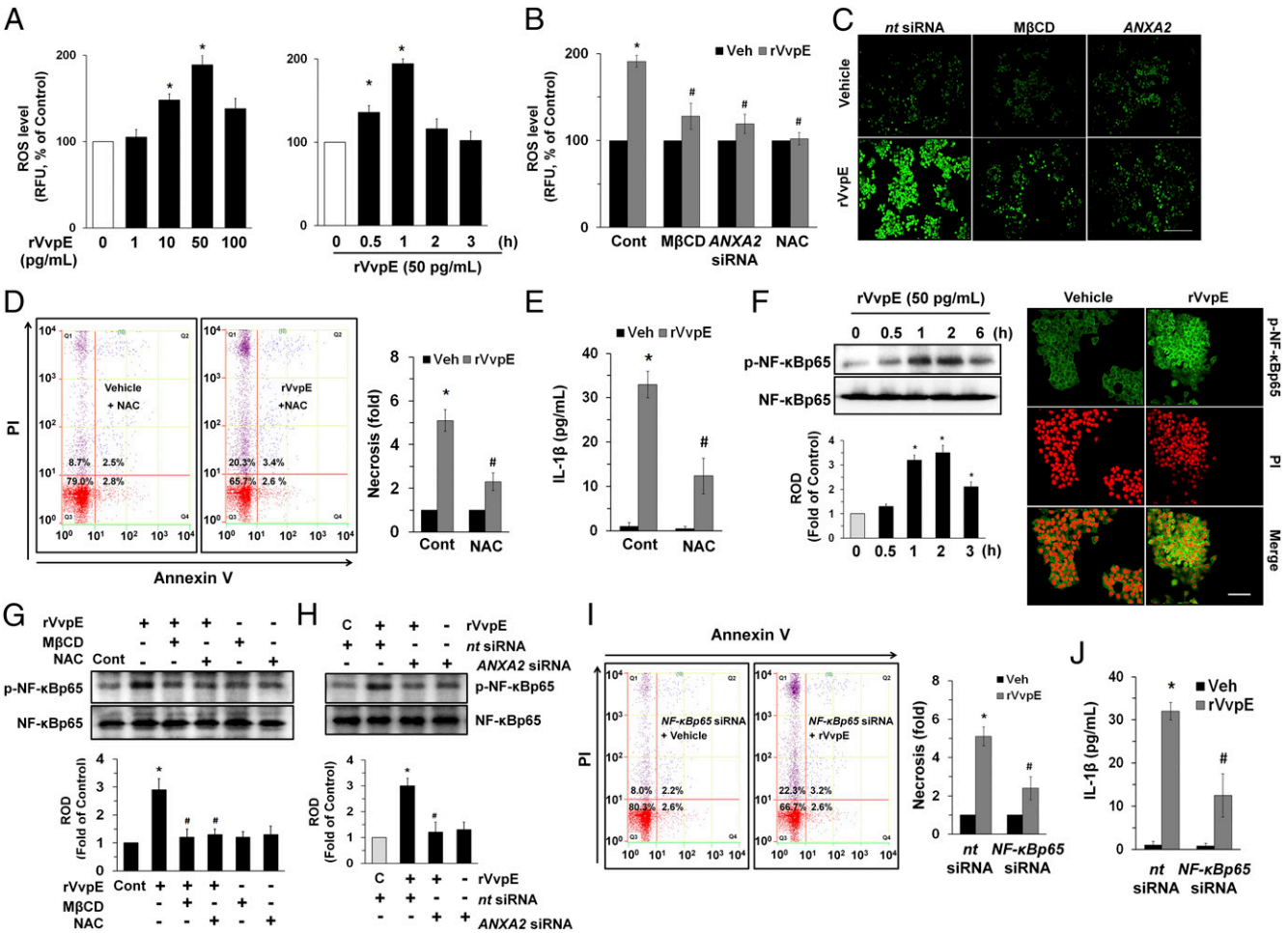

FIGURE 3. Regulatory effect of VvpE on ROS production and NF-κB phosphorylation. (**A**) Dose responses of rVvpE for 1 h (*left panel*) and time responses of 50 pg/ml rVvpE (*right panel*) in ROS production are shown. $n = 4$. Cells were transfected with *ANXA2* siRNA for 24 h or pretreated with MβCD (0.1 mM) and NAC (10 μM) prior to rVvpE exposure for 1 h. (**B**) The level of ROS production is shown. $n = 4$. (**C**) ROS production (green) was visualized by confocal microscopy. Scale bars, 100 μm. $n = 3$. Cells were pretreated with NAC prior to rVvpE exposure for 6 h. (**D**) FACS analysis and quantitative analysis of the percentage of necrotic (Q1) cells are shown. $n = 4$. (**E**) The level of IL-1β protein was quantified by ELISA. $n = 5$. (**F**) Time responses of rVvpE in the phosphorylation of NF-κBp65 are shown (*left panel*). p–NF-κBp65 (green) was detected by immunostaining with p–NF-κBp65 Ab in cells treated with rVvpE for 2 h (right panel). Scale bars, 50 μm (original magnification ×400). PI was used for nuclear counterstaining (red). $n = 3$. (**G**) Cells were pretreated with MβCD or NAC prior to rVvpE exposure for 2 h. The phosphorylation of NF-κBp65 is shown. $n = 4$. (**H**) Cells were transfected with *ANXA2* siRNA prior to rVvpE exposure for 2 h. The phosphorylation of NF-κBp65 is shown. $n = 4$. INT-407 cells transfected with *NF-κBp65* siRNA were incubated with rVvpE (50 pg/ml) for 6 h. (**I**) FACS analysis and quantitative analysis of the percentage of necrotic (Q1) cells are shown. $n = 4$. (**J**) The level of IL-1β protein was quantified by ELISA. $n = 5$. (A, B, and D–J) Data represent mean ± SEM. $^*p < 0.01$ versus control, vehicle alone, or nontargeting siRNA plus vehicle. $^\#p < 0.05$ versus rVvpE. Cont, control; Veh, vehicle.

NAC (Fig. 3G) as well as knockdown of ANXA2 (Fig. 3H). These data represent evidence that the phosphorylation of NF-κBp65 is regulated by ROS produced by the clustering of NOX enzymes and ANXA2 in membrane lipid rafts. Knockdown of NF-κBp65 by siRNA also showed a significant inhibitory effect on the necrotic cell death (Fig. 3I) as well as the production of IL-1β (Fig. 3J) in INT-407 cells.

Regulatory effect of VvpE on the interaction of NF-κB with the IL-1β promoter

To determine whether NF-κB directly regulates *IL-1β* mRNA expression, we performed *IL-1β* promoter region analysis using Alggen Promo (28, 29). The *IL-1β* promoter located between the transcription start site and −500 bp upstream contains two putative NF-κB binding sites and three methylation sites, including one site that was placed next to methylation sites (Fig. 4A). We first performed a ChIP assay followed by qRT-PCR in INT-407 cells treated with rVvpE to determine the regulatory effect of VvpE on the binding of NF-κB to the *IL-1β* promoter. We tested two sets of primers that include two putative NF-κB binding sites at the region proximal to −500 bp of the start site of the *IL-1β* promoter. We found that all primer sets result in an amplicon from the anti–pNF-κB65 immunoprecipitates, and, importantly that the interaction of NF-κB with the *IL-1β* promoter was enhanced by the rVvpE treatment in only the primer set ranging between −347 and −174 bp (Fig. 4B). Interestingly, however, the level of NF-κB binding to the *IL-1β* promoter was significantly inhibited by knockdown of ANXA2 and by pretreatment with the MβCD and NAC (Fig. 4C, 4D). These results suggest that rVvpE transcriptionally regulates the NF-κB binding to the unique region of the *IL-1β* promoter, which was regulated by necrotic signaling pathway as well as inflammation. Because of the inhibitory role of promoter methylation on the gene transcription, we postulated that rVvpE could affect the methylations, which negatively regulate the interaction of NF-κB with the *IL-1β* promoter. We determined the methylation status following the treatment with rVvpE by means of MSP. A bisulfite treatment converted cytosine residues in the genomic DNA to uracil, which were amplified as thymine during the subsequent PCR. We attempted to analyze the methylation status of the *IL-1β* gene promoter at −299 CpG sites due to their close distance to putative NF-κB binding sites. As shown in Fig. 4E, primers for −299 CpG sites that specifically amplified either the methylated or unmethylated form of the *IL-1β* promoter produced 100-bp methylated bands from vehicle-treated INT-407 cells, indicating that the *IL-1β* promoter was methylated in these alleles. However, treatment with 50 pg/ml rVvpE for 2 h markedly inhibited the level of *IL-1β* promoter methylation, which was significantly blocked by knockdown of *ANXA2* and by pretreatment with the MβCD and NAC. Interestingly, the levels of the phosphorylation of NF-κBp65 (Fig. 4F) and production of IL-1β (Fig. 4G) were markedly enhanced by pretreatment with the DNA methylation inhibitor 5-Aza. These data indicate that the hypomethylation of the *IL-1β* promoter is able to affect the high level of the interaction of NF-κB with the *IL-1β* promoter during necrotic cell death evoked by rVvpE. *V. vulnificus* was known to stimulate the activation of caspase-1 and IL-1β via the NLRP3 inflammasome, which is one member of NLR (38). Similar to the previous report (38), an increase in active forms of IL-1β (17 kDa) and caspase-1 (10 kDa) was observed after 6 h of incubation with 50 pg/ml rVvpE (Fig. 4H). However, the activation of IL-1β by rVvpE was markedly inhibited by transfection with siRNAs for *NLRP3* and *caspase-1* (Fig. 4I). Thus, these results indicate that rVvpE has the ability to induce pyroptosis accompanied by NLRP3-mediated caspase-1 activation that results in maturation of IL-1β.

Essential role of VvpE in promoting inflammation-related intestinal injury

To evaluate the functional relevance of *V. vulnificus* VvpE, 7-wk-old ICR mice were inoculated i.g. with boiled *V. vulnificus* (control), *V. vulnificus* (WT), and a mutant deficient in *vvpE* gene in *V. vulnificus* (*vvpE* mutant) at 1.1×10^6 CFU/ml for 18 h, after which the level of bacterial colonization was monitored. The WT colonization in ileum increased by 3.2 ± 0.3 ($\times 10^6$ CFU/g tissue) (Fig. 5A). However, when the mice were inoculated with *vvpE* mutant, the levels were diminished by 2.4 ± 0.2 ($\times 10^6$ CFU/g tissue), compared with the WT. We found that all of the mice given oral administrations of WT had survived by 18 h postinjection (data not shown). These results indicate that VvpE contributes to the intestinal colonization of *V. vulnificus* in vivo. We further found that WT strongly induces the phosphorylation of NF-κBp65 (Fig. 5B) and the expression of proinflammatory cytokines, including IL-1β, IL-6, and TNF-α (Fig. 5C) in the mouse intestine. However, unlike WT, the mice infected with *vvpE* mutant almost completely maintained the levels of NF-κBp65 phosphorylation and proinflammatory cytokines to the normal level. These results indicate that VvpE is a critical elastase that promotes intestinal inflammatory responses. In response to an inflammation-related injury, intestinal epithelial cells at the wound edge proliferate and migrate to cover denuded surfaces and re-establish the critical barrier function (39). Thus, we have further investigated whether VvpE also has a virulence effect on cell proliferation during inflammatory processes. We found that the number of proliferating cells identified by Ki67 labeling was significantly decreased in the intestinal crypt of mice infected with WT compared with control mice (Fig. 5D). However, the cytotoxic effect of WT was negated by infection with the *vvpE* mutant, suggesting that VvpE regulates host cell death as well as inflammatory response in intestinal epithelial cells. To assess the level of enterocyte migration, BrdU pulse chase experiments were performed in mice inoculated i.g. with control, WT, or *vvpE* mutant at 1.1×10^6 CFU/ml for 18 h (Fig. 5E). Two hours after the BrdU injection, BrdU-labeled intestinal epithelial cells of control mice were located at the bottom of the ileum crypt. Subsequently, the cells migrated upward and moved farther along the crypt villus axis, reaching about two thirds of the location of the villi at 48 h. In comparison, mice infected with WT had fewer $BrdU^+$ intestinal epithelial cells present at the ileum crypt and showed a reduced rate of migration compared with the control. Interestingly, the mice that received the *vvpE* mutant were still keeping the migratory behavior of intestinal epithelial cells at physiological levels. Thus, these results indicate that VvpE plays an important role in inflammation-related injury related to cell proliferation and migration in intestinal epithelial cells. To verify the role of VvpE in wound recovery, we further examined the ability of 50 pg/ml rVvpE to regulate cell motility for 6 h using an in vitro wound-healing migration assay. As shown in Fig. 5F, 1% FBS significantly induced cell motility of INT-407 cells. In contrast, the cell migration–promoting activity of FBS was attenuated by a rVvpE treatment. We also visualized the ability of VvpE to regulate cell motility by staining the cells with calcein AM in an Oris cell migration assay (Fig. 5G). In contrast to the control, 1% FBS significantly induced the translocation of cell bodies into the denuded area for wound healing, which was inhibited by a rVvpE treatment. Additionally, Fig. 5H shows that rVvpE inhibited FBS-induced cell migration, but this effect was silenced by the knockdown of the expression of ANXA2, but not by ANXA4.

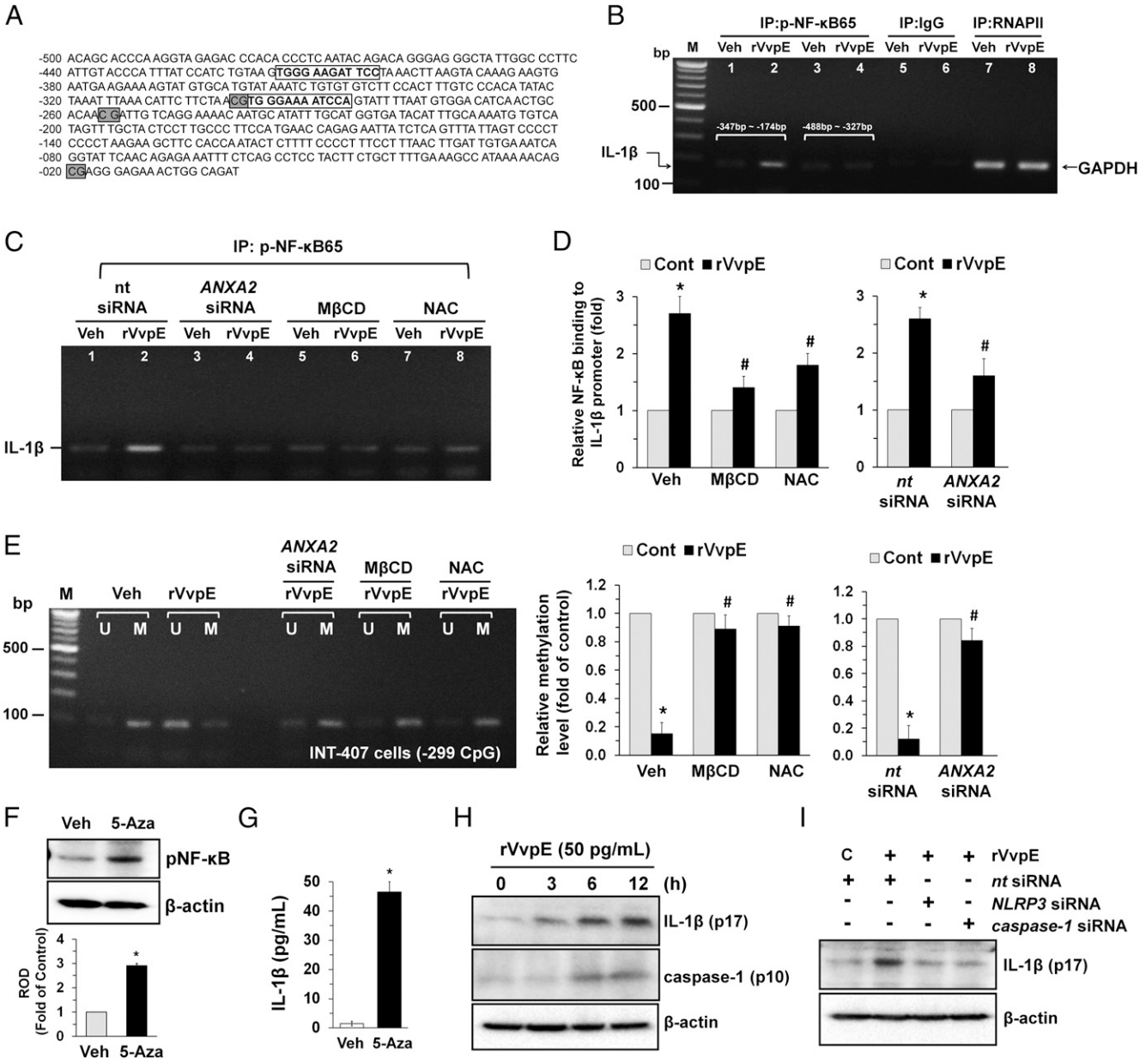

FIGURE 4. Regulatory effect of VvpE on the interaction of NF-κB with the *IL-1β* promoter. (**A**) The sites for NF-κB binding and methylaton in the *IL-1β* promoter are shown. The open boxes and shaded boxes represent the consensus sequences of NF-κB and the methylation site, respectively. (**B**) INT-407 cells treated with rVvpE for 2 h were fixed with formaldehyde, and cell extracts were immunoprecipitated (IP) with anti-p–NF-κBp65 to detect bound *IL-1β* promoter DNA fragments (−347 to –174 or −488 to −327 bp). A representative agarose gel following RT-PCR is shown. $n = 3$. Normal mouse IgG or anti-RNA polymerase II Ab was used as negative or positive control for the ChIP, respectively. (**C**) Cells were transfected with *ANXA2* siRNA or pretreated with MβCD or NAC prior to rVvpE (50 pg/ml) exposure for 2 h. The binding of p–NF-κBp65 to *IL-1β* promoter was determined by ChIP. A representative agarose gel following RT-PCR is shown. $n = 3$. (**D**) The level of p–NF-κBp65 binding to *IL-1β* promoter was quantified by qRT-PCR. Anti-RNA polymerase II Ab was used internal control. $n = 4$. (**E**) Genomic DNA of the cells transfected with *ANXA2* siRNA or pretreated with MβCD or NAC prior to rVvpE (50 pg/ml) exposure for 2 h was prepared. Changes in the *IL-1β* promoter methylation status at −299 CpG site was determined by MSP analysis (*left panel*). The relative level of *IL-1β* methylation is shown, compared with the unmethylated form (*right panel*). $n = 4$. The phosphorylation of NF-κBp65 (**F**) and the production of IL-1β (**G**) in cells pretreated with 5-Aza (1 μM) for 30 min prior to rVvpE exposure are shown. (**H**) Time responses of 50 pg/ml rVvpE in expression of active IL-1β and cleaved caspase-1 are shown. $n = 3$. (**I**) Cells were transfected with *NLRP* and *caspase-1* siRNAs prior to rVvpE (50 pg/ml) exposure for 6 h. The expression of active IL-1β is shown. $n = 3$. (D–G) Data represent mean ± SEM. $^{*}p < 0.05$ versus vehicle alone or nontargeting siRNA plus vehicle. $^{\#}p < 0.05$ versus rVvpE. Veh, vehicle.

Discussion

Our data in the present study demonstrate that VvpE is the functional elastase of *V. vulnificus* that stimulates IL-1β secretion by means of hypomethylation and NF-κB activation via lipid raft–dependent ANXA2 recruitment and ROS signaling during the pyroptosis of intestinal epithelial cells. The mechanism and outcome of pyroptosis are distinctly different from these aspects of apoptosis, which actively inhibit inflammation. We showed that rVvpE induces pyroptotic cell death coupled with the production of IL-1β via lipid rafts. These findings differed from those previously reported and revealed that the effect of that VvhA, one of the major toxins of *V. vulnificus*, on cytotoxicity is independent of the action of lipid rafts (40). Thus, the results of our present study suggest that *V. vulnificus* uniquely regulates intestinal cell death and inflammation by producing the VvpE with modes of action that differ from those of other secreted proteins. In fact, many

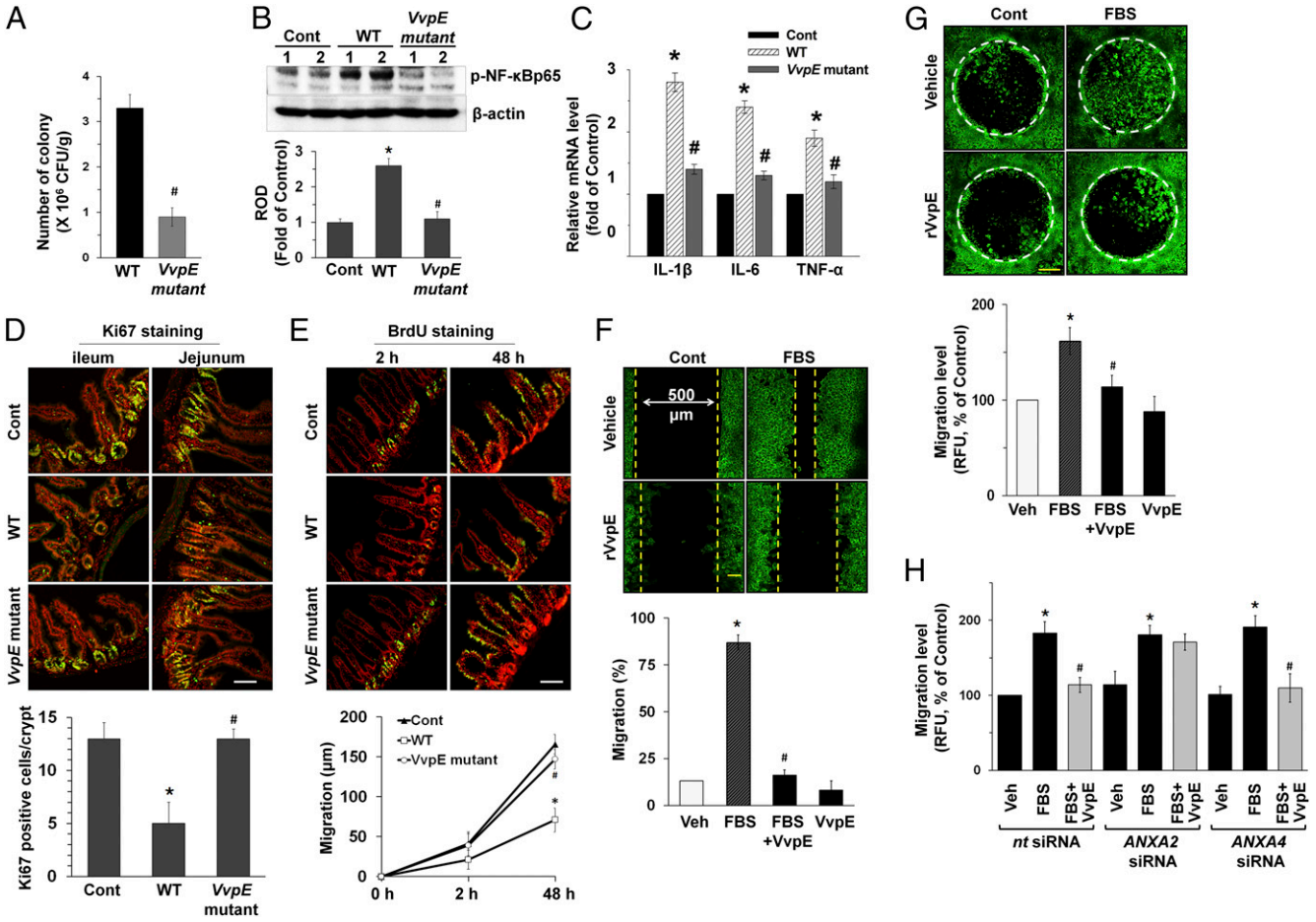

FIGURE 5. Essential role of VvpE in promoting inflammation-related intestinal injury. (**A**) Mice ($n = 10$) were received i.g. inoculation of boiled *V. vulnificus* (control), *V. vulnificus* (WT), and a mutant deficient in *vvpE* gene in *V. vulnificus* (*vvpE* mutant) for 18 h and sacrificed. Note that the mice were given BrdU (50 mg/kg) by i.p. injections for 2 or 48 h prior to the sacrifice. Colonization activities in ileum tissue were determined. $n = 10$. (**B**) The phosphorylation level of NF-κBp65 and (**C**) the expression levels of proinflammatory cytokines (IL-1β, IL-6, and TNF-α) in ileum tissue are shown. (**D**) Expression of Ki67 (green) in ileum and jejunum was examined by confocal microscopy. PI was used for nuclear counterstaining (red). Scale bar, 100 μm (original magnification ×200). The mean numbers of Ki67-labeled cells per crypt are shown in the bar graph (bottom panel). $n = 5$. (**E**) Migration of proliferating enterocytes along the crypt/villus axis was determined by BrdU pulse-chase for indicated times in ileum. The extent of cell migration was quantified by measuring the distance between the crypt base and the highest labeled cell along the crypt-villus axis. Scale bars, 100 μm (original magnification ×200). $n = 5$. (**F**) Migration of INT-407 cells cotreated with rVvpE (50 pg/ml) and 1% FBS into the nude area at 6 h is shown. Cell migration was measured by using wound-healing migration assay. The extent of wound closure was quantified. Full recovery of the wound was considered as 100%. $n = 3$. (**G**) Migration of cells cotreated with rVvpE (50 pg/ml) and 1% FBS from cell seeding zone to detection zone was measured by using Oris cell migration assay. $n = 3$. Scale bar, 100 μm. (**H**) Cells transfected with siRNAs for nontargeting (nt) control, ANXA2, and ANXA4 were coincubated with rVvpE (50 pg/ml) and 1% FBS for 6 h. Cell migration was measured by using Oris cell migration assay. $n = 3$. (B–E) Data represent mean ± SEM. $^{*}p < 0.05$ versus control, $p < 0.05$ versus WT. (F–H) Data represent mean ± SEM. $^{*}p < 0.01$ versus vehicle. $^{\#}p < 0.05$ versus 1% FBS alone.

studies have reported that several enteric bacterial pathogens, including *H. pylori* vacuolating toxins (41) and the enterotoxin *Clostridium perfringens* (42), may interact with a detergent-resistant cellular membrane composed of relatively abundant cholesterol as an initial attachment platform and therefore having a cytotoxic effect on intestinal physiological functions. Therefore, the findings in the present study suggest that lipid rafts are a functional mediator that initiates the virulence effect of rVvpE to induce host cell death as well as inflammation. Concerning the pathogenic mechanism of VvpE, we subsequently showed the unique involvement of lipid raft–dependent ANXA2 recruitment and ROS production in the regulation of IL-1β secretion during pyroptotic cell death. The importance of ANXA2 in microbial pathogenesis is underscored by the finding that *E. coli* (*EPEC*) adherence induces the concentration of cholesterol and GPI-anchored proteins at sites of bacterial contact, where ANXA2 is recruited to the cytoplasmic membrane surface, possibly stabilizing raft patches and their links to the actin cytoskeleton beneath adhering to EPEC (34). Thus, these results present the possibility that rVvpE influences the structure and localization of ANXA2 through lipid rafts to promote proinflammatory signaling in intestinal epithelial cells. Compelling evidence further supported the critical role of ANXA2 in inflammatory myopathies (43) as well as in inflammatory bowel disease (44). Taken together, our finding that VvpE induces proinflammatory responses via an ANXA2-dependent mechanism provides information about the important mechanisms of pathogen-induced cell death during *V. vulnificus* infection. Increasing evidence has suggested that lipid rafts are clustered to form a redox signaling platform through $gp91^{phox}$ (NOX2) coupling with cytosolic factors that include $p47^{phox}$ (NCF1), $p67^{phox}$ (NCF2), and small GTPase Rac1 (45-47), and that these processes subsequently produce superoxides and other ROS (45). Although in most cell types, mitochondrial ROS are thought to be the largest contributor to intracellular ROS production (48), our result showed that the sequestration of cholesterol by MβCD attenuates intracellular ROS production and

pyroptotic cell death induced by rVvpE. Hence, the current findings further indicate that epithelial ROS generated by NOX within lipid rafts may influence on the mitochondrial ROS production and thereby contribute to increased total intracellular ROS generation, leading to pyroptotic cell death.

The ROS generated by a bacterial infection have been shown to induce the oxidative inactivation of several proteins harboring oxidant-sensitive thiol groups and of the ubiquitin–proteasome pathway (16), thereby activating many redox-sensitive proteins that include regulators of MAPK pathways and focal adhesion kinase, as well as several components involved in NF-κB activation (16). NF-κB is one of the master oxidative transcriptional regulators of the host inflammatory signaling pathway and the cell death pathway in response to bacterial pathogens by inducing the expression of a proinflammatory mediator that orchestrates and sustains the inflammatory response and causes tissue damage (1, 16). We found that rVvpE can induce the phosphorylation of NF-κB through ROS production and that the inhibition of NF-κB blocks rVvpE-induced cell death. Regarding the role of ROS in NF-κB activation, earlier work showed that the JNK pathway induced by ROS can influence NF-κB activation in promoting apoptotic cell death (49). Additionally, pERK1/2 was reported to have the ability to translocate into the nucleus, where it phosphorylates various substrates, such as transcriptional factors, thereby transmitting the signals received by cell surface receptors to the nucleus (50). Hence, it is conceivable that ROS induced by rVvpE have a potential role in promoting the NF-κB pathway through the activation of ERK1/2 and JNK. Based on these results, we suggest that rVvpE stimulates ROS-mediated NF-κB activation in promoting the cell death of INT-407 cells. Whereas the NF-κB binding activity of the *IL-1β* gene promoter is the critical mechanism of the transcriptional regulation of *IL-1β*, the promoter methylation of cytosine residues at CpG dinucleotides is also an important posttranslational modification affecting NF-κB transcription. The important finding of this study is that rVvpE uniquely regulates the interaction between NF-κB and the *IL-1β* promoter at the region between –297 and −286 bp upstream of the transcription start while also inhibiting the methylation status of the *IL-1β* gene promoter at the −299 CpG site, located immediately before the −297 bp site occupied by NF-κB. It is not clear whether the regulatory effect of rVvpE in promoting the interaction between NF-κB and the *IL-1β* promoter is a sequential result of the hypomethylation of *IL-1β* promoter or, alternatively, an independent process involving other cellular signaling events. Although the effects of ROS on epigenetic modulation are still poorly understood, it was clearly shown that ROS induced by a H_2O_2 treatment regulate histone acetyltransferases and deacetylases, the key enzymes responsible for chromatin remodeling, suggesting that posttranslational modifications affecting NF-κB are also redox sensitive (51). Indeed, our data revealed that hypomethylation by 5-Aza is closely related to high level of the NF-κB activation and to IL-1β secretion. These data provide, to our knowledge, the first evidence that a bacterial pathogen induces the hypomethylation of the *IL-1β* promoter as well as the transcriptional regulation of NF-κB to promote IL-1β production during host cell death.

Given current in vitro observations that IL-1β production is a hallmark of necrosis evoked by rVvpE, our in vivo study shows that VvpE is an important secreted virulence factor of *V. vulnificus* responsible for the inflammatory response, which stimulates NF-κB activation and proinflammatory cytokine expression. Although there are many limiting factors to understand why VvpE mutant completely inhibits the NF-κB activation and proinflammatory cytokine expression, it is possible that the VvpE would affect the delivery of major toxins (e.g., *VvhA, MARTXVv*) for NF-κB activation during intestinal infection of *V. vulnificus.* Alternatively, exacerbation of the inflammatory response in the intestine may reflect the altered proliferation and migration of intestinal epithelial cells during intestinal wound repair (39). Similarly, a previous study showed that an intestinal infection of *H. pylori* inhibits cell proliferation without affecting cell migration, thereby delaying wound healing in intestinal inflammatory injuries (52). However, the role of VvpE in promoting inflammation-related events is not yet well understood. The salient finding of this study is that VvpE is a functional elastase delaying the upward movement of enterocytes along the crypt/villus axis while also impairing enterocyte proliferation at the crypt part. These data further indicate that severe inflammation mediated by VvpE may interfere with epithelial cell migration and proliferation and that this may inhibit the reestablishment of the intestinal barrier function. In support of these findings, our in vitro results, verifying that rVvpE inhibits serum-induced cell migration via an ANXA2-dependent mechanism, provides good evidence that necrotic cell death may result in a delay of wound recovery by rVvpE. Indeed, an earlier study suggested that the silencing of ANXA2 enhances the proliferation of colon epithelial cells and ameliorates gut inflammation, improving intestinal mucosal wound repair (44). Hence, we suggest that ANXA2 plays a critical role as a host mediator of VvpE and that it has unique biological properties responsible for host cell death coupled with an inflammatory response.

In conclusion, our results suggest that rVvpE induces NF-κB–dependent IL-1β production via lipid raft–dependent ANXA2 recruitment and ROS production in intestinal epithelial cells. Thus, highlighting the signaling pathways involved in the rVvpE-stimulated cell death pathway may provide potential therapeutic targets for strategic modulations of *V. vulnificus* infections.

Disclosures

The authors declare no conflict of interest.

References

1. Ashida, H., M. Ogawa, M. Kim, H. Mimuro, and C. Sasakawa. 2012. Bacteria and host interactions in the gut epithelial barrier. *Nat. Chem. Biol.* 8: 36–45.
2. Fink, S. L., and B. T. Cookson. 2005. Apoptosis, pyroptosis, and necrosis: mechanistic description of dead and dying eukaryotic cells. *Infect. Immun.* 73: 1907–1916.
3. Blake, P. A., M. H. Merson, R. E. Weaver, D. G. Hollis, and P. C. Heublein. 1979. Disease caused by a marine *Vibrio*. Clinical characteristics and epidemiology. *N. Engl. J. Med.* 300: 1–5.
4. Park, S. D., H. S. Shon, and N. J. Joh. 1991. *Vibrio vulnificus* septicemia in Korea: clinical and epidemiologic findings in seventy patients. *J. Am. Acad. Dermatol.* 24: 397–403.
5. Jeong, H. G., and K. J. Satchell. 2012. Additive function of *Vibrio vulnificus* MARTX(Vv) and VvhA cytolysins promotes rapid growth and epithelial tissue necrosis during intestinal infection. *PLoS Pathog.* 8: e1002581.
6. Lee, J. H., M. W. Kim, B. S. Kim, S. M. Kim, B. C. Lee, T. S. Kim, and S. H. Choi. 2007. Identification and characterization of the *Vibrio vulnificus* rtxA essential for cytotoxicity in vitro and virulence in mice. *J. Microbiol.* 45: 146–152.
7. Miyoshi, S. 2006. *Vibrio vulnificus* infection and metalloprotease. *J. Dermatol.* 33: 589–595.
8. Kothary, M. H., and A. S. Kreger. 1987. Purification and characterization of an elastolytic protease of *Vibrio vulnificus. J. Gen. Microbiol.* 133: 1783–1791.
9. Miyoshi, S., and S. Shinoda. 1992. Activation mechanism of human Hageman factor-plasma kallikrein-kinin system by *Vibrio vulnificus* metalloprotease. *FEBS Lett.* 308: 315–319.
10. Molla, A., T. Yamamoto, T. Akaike, S. Miyoshi, and H. Maeda. 1989. Activation of hageman factor and prekallikrein and generation of kinin by various microbial proteinases. *J. Biol. Chem.* 264: 10589–10594.
11. Jeong, K. C., H. S. Jeong, J. H. Rhee, S. E. Lee, S. S. Chung, A. M. Starks, G. M. Escudero, P. A. Gulig, and S. H. Choi. 2000. Construction and phenotypic evaluation of a *Vibrio vulnificus* vvpE mutant for elastolytic protease. *Infect. Immun.* 68: 5096–5106.
12. Jones, M. K., and J. D. Oliver. 2009. *Vibrio vulnificus*: disease and pathogenesis. *Infect. Immun.* 77: 1723–1733.

13. Kim, H. Y., A. K. Chang, J. E. Park, I. S. Park, S. M. Yoon, and J. S. Lee. 2007. Procaspase-3 activation by a metalloprotease secreted from *Vibrio vulnificus*. *Int. J. Mol. Med.* 20: 591–595.
14. Kim, C. M., R. Y. Park, H. J. Chun, S. Y. Kim, J. H. Rhee, and S. H. Shin. 2007. *Vibrio vulnificus* metalloprotease VvpE is essentially required for swarming. *FEMS Microbiol. Lett.* 269: 170–179.
15. Ashida, H., H. Mimuro, M. Ogawa, T. Kobayashi, T. Sanada, M. Kim, and C. Sasakawa. 2011. Cell death and infection: a double-edged sword for host and pathogen survival. *J. Cell Biol.* 195: 931–942.
16. Neish, A. S. 2013. Redox signaling mediated by the gut microbiota. *Free Radic. Res.* 47: 950–957.
17. Paesold, G., D. G. Guiney, L. Eckmann, and M. F. Kagnoff. 2002. Genes in the *Salmonella* pathogenicity island 2 and the *Salmonella* virulence plasmid are essential for *Salmonella*-induced apoptosis in intestinal epithelial cells. *Cell. Microbiol.* 4: 771–781.
18. Jones, R. M., H. Wu, C. Wentworth, L. Luo, L. Collier-Hyams, and A. S. Neish. 2008. *Salmonella* AvrA coordinates suppression of host immune and apoptotic defenses via JNK pathway blockade. *Cell Host Microbe* 3: 233–244.
19. Ki, M. R., H. R. Lee, M. J. Goo, I. H. Hong, S. H. Do, D. H. Jeong, H. J. Yang, D. W. Yuan, J. K. Park, and K. S. Jeong. 2008. Differential regulation of ERK1/2 and p38 MAP kinases in VacA-induced apoptosis of gastric epithelial cells. *Am. J. Physiol. Gastrointest. Liver Physiol.* 294: G635–G647.
20. Nougayrède, J. P., and M. S. Donnenberg. 2004. Enteropathogenic *Escherichia coli* EspF is targeted to mitochondria and is required to initiate the mitochondrial death pathway. *Cell. Microbiol.* 6: 1097–1111.
21. Takahashi, K. 2014. Influence of bacteria on epigenetic gene control. *Cell. Mol. Life Sci.* 71: 1045–1054.
22. Lee, B. C., M. S. Kim, D. Cho, S. H. Choi, and T. S. Kim. 2010. Co-culture supernatants from *Vibrio vulnificus*-infected INT-407 cells induce IL-8 production in intestinal epithelial cells: crucial role of *V. vulnificus* rtxE. *Int. J. Mol. Med.* 26: 651–659.
23. Lee, B. C., J. H. Lee, M. W. Kim, B. S. Kim, M. H. Oh, K. S. Kim, T. S. Kim, and S. H. Choi. 2008. *Vibrio vulnificus* rtxE is important for virulence, and its expression is induced by exposure to host cells. *Infect. Immun.* 76: 1509–1517.
24. Lee, K. J., N. Y. Lee, Y. S. Han, J. Kim, K. H. Lee, and S. J. Park. 2010. Functional characterization of the IlpA protein of *Vibrio vulnificus* as an adhesin and its role in bacterial pathogenesis. *Infect. Immun.* 78: 2408–2417.
25. Kim, S. M., J. H. Park, H. S. Lee, W. B. Kim, J. M. Ryu, H. J. Han, and S. H. Choi. 2013. LuxR homologue SmcR is essential for *Vibrio vulnificus* pathogenesis and biofilm detachment, and its expression is induced by host cells. *Infect. Immun.* 81: 3721–3730.
26. Brett, C. M., C. B. Washington, R. J. Ott, M. M. Gutierrez, and K. M. Giacomini. 1993. Interaction of nucleoside analogues with the sodium-nucleoside transport system in brush border membrane vesicles from human kidney. *Pharm. Res.* 10: 423–426.
27. Lee, S. J., Y. H. Jung, S. Y. Oh, S. P. Yun, and H. J. Han. 2014. Melatonin enhances the human mesenchymal stem cells motility via melatonin receptor 2 coupling with Gαq in skin wound healing. *J. Pineal Res.* 57: 393–407.
28. Messeguer, X., R. Escudero, D. Farré, O. Núñez, J. Martínez, and M. M. Albà. 2002. PROMO: detection of known transcription regulatory elements using species-tailored searches. *Bioinformatics* 18: 333–334.
29. Farré, D., R. Roset, M. Huerta, J. E. Adsuara, L. Roselló, M. M. Albà, and X. Messeguer. 2003. Identification of patterns in biological sequences at the ALGGEN server: PROMO and MALGEN. *Nucleic Acids Res.* 31: 3651–3653.
30. Chieng-Yane, P., A. Bocquet, R. Létienne, T. Bourbon, S. Sablayrolles, M. Perez, S. N. Hatem, A. M. Lompré, B. Le Grand, and M. David-Dufilho. 2011. Protease-activated receptor-1 antagonist F 16618 reduces arterial restenosis by down-regulation of tumor necrosis factor α and matrix metalloproteinase 7 expression, migration, and proliferation of vascular smooth muscle cells. *J. Pharmacol. Exp. Ther.* 336: 643–651.
31. Park, J. H., and H. J. Han. 2009. Caveolin-1 plays important role in EGF-induced migration and proliferation of mouse embryonic stem cells: involvement of PI3K/Akt and ERK. *Am. J. Physiol. Cell Physiol.* 297: C935–C944.
32. Burkart, A., B. Samii, S. Corvera, and H. S. Shpetner. 2003. Regulation of the SHP-2 tyrosine phosphatase by a novel cholesterol- and cell confluence-dependent mechanism. *J. Biol. Chem.* 278: 18360–18367.
33. Rescher, U., and V. Gerke. 2004. Annexins—unique membrane binding proteins with diverse functions. *J. Cell Sci.* 117: 2631–2639.
34. Zobiack, N., U. Rescher, S. Laarmann, S. Michgehl, M. A. Schmidt, and V. Gerke. 2002. Cell-surface attachment of pedestal-forming enteropathogenic *E. coli* induces a clustering of raft components and a recruitment of annexin 2. *J. Cell Sci.* 115: 91–98.
35. Lin, L. L., C. N. Chen, W. C. Lin, P. H. Lee, K. J. Chang, Y. P. Lai, J. T. Wang, and H. F. Juan. 2008. Annexin A4: A novel molecular marker for gastric cancer with *Helicobacter pylori* infection using proteomics approach. *Proteomics Clin. Appl.* 2: 619–634.
36. Kashimoto, T., S. Ueno, H. Ehara, S. Fukudome, M. Komai, and N. Susa. 2009. Oligomerization is essential for apoptotic activity of *Vibrio vulnificus* hemolysin. *J. Vet. Med. Sci.* 71: 1403–1406.
37. Zhang, C., J. J. Hu, M. Xia, K. M. Boini, C. Brimson, and P. L. Li. 2010. Redox signaling via lipid raft clustering in homocysteine-induced injury of podocytes. *Biochim. Biophys. Acta* 1803: 482–491.
38. Toma, C., N. Higa, Y. Koizumi, N. Nakasone, Y. Ogura, A. J. McCoy, L. Franchi, S. Uematsu, J. Sagara, S. Taniguchi, et al. 2010. Pathogenic *Vibrio* activate NLRP3 inflammasome via cytotoxins and TLR/nucleotide-binding oligomerization domain-mediated NF-κB signaling. *J. Immunol.* 184: 5287–5297.
39. Ivanov, A. I., C. A. Parkos, and A. Nusrat. 2010. Cytoskeletal regulation of epithelial barrier function during inflammation. *Am. J. Pathol.* 177: 512–524.
40. Sugiyama, H., T. Kashimoto, S. Ueno, H. Ehara, T. Kodama, T. Iida, and N. Susa. 2011. Relationship between localization on cellular membranes and cytotoxicity of *Vibrio vulnificus* hemolysin. *PLoS One* 6: e26018.
41. Fassino, S., D. Svrakic, G. Abbate-Daga, P. Leombruni, F. Amianto, S. Stanic, and G. G. Rovera. 2002. Anorectic family dynamics: temperament and character data. *Compr. Psychiatry* 43: 114–120.
42. van der Goot, F. G., and T. Harder. 2001. Raft membrane domains: from a liquid-ordered membrane phase to a site of pathogen attack. *Semin. Immunol.* 13: 89–97.
43. Probst-Cousin, S., C. Berghoff, B. Neundörfer, and D. Heuss. 2004. Annexin expression in inflammatory myopathies. *Muscle Nerve* 30: 102–110.
44. Tsukamoto, H., S. Tanida, K. Ozeki, M. Ebi, T. Mizoshita, T. Shimura, Y. Mori, H. Kataoka, T. Kamiya, S. Fukuda, et al. 2013. Annexin A2 regulates a disintegrin and metalloproteinase 17-mediated ectodomain shedding of pro-tumor necrosis factor-α in monocytes and colon epithelial cells. *Inflamm. Bowel Dis.* 19: 1365–1373.
45. Li, P. L., Y. Zhang, and F. Yi. 2007. Lipid raft redox signaling platforms in endothelial dysfunction. *Antioxid. Redox Signal.* 9: 1457–1470.
46. Kusumoto, K., T. Kawahara, Y. Kuwano, S. Teshima-Kondo, K. Morita, K. Kishi, and K. Rokutan. 2005. Ecabet sodium inhibits *Helicobacter pylori* lipopolysaccharide-induced activation of NADPH oxidase 1 or apoptosis of guinea pig gastric mucosal cells. *Am. J. Physiol. Gastrointest. Liver Physiol.* 288: G300–G307.
47. Zhang, D. X., A. P. Zou, and P. L. Li. 2003. Ceramide-induced activation of NADPH oxidase and endothelial dysfunction in small coronary arteries. *Am. J. Physiol. Heart Circ. Physiol.* 284: H605–H612.
48. Holmström, K. M., and T. Finkel. 2014. Cellular mechanisms and physiological consequences of redox-dependent signalling. *Nat. Rev. Mol. Cell Biol.* 15: 411–421.
49. Seo, B. N., J. M. Ryu, S. P. Yun, J. H. Jeon, S. S. Park, K. B. Oh, J. K. Park, and H. J. Han. 2013. Delphinidin prevents hypoxia-induced mouse embryonic stem cell apoptosis through reduction of intracellular reactive oxygen species-mediated activation of JNK and NF-κB, and Akt inhibition. *Apoptosis* 18: 811–824.
50. Lidke, D. S., F. Huang, J. N. Post, B. Rieger, J. Wilsbacher, J. L. Thomas, J. Pouysségur, T. M. Jovin, and P. Lenormand. 2010. ERK nuclear translocation is dimerization-independent but controlled by the rate of phosphorylation. *J. Biol. Chem.* 285: 3092–3102.
51. Rahman, I., J. Marwick, and P. Kirkham. 2004. Redox modulation of chromatin remodeling: impact on histone acetylation and deacetylation, NF-κB and pro-inflammatory gene expression. *Biochem. Pharmacol.* 68: 1255–1267.
52. Ricci, V., C. Ciacci, R. Zarrilli, P. Sommi, M. K. Tummuru, C. Del Vecchio Blanco, C. B. Bruni, T. L. Cover, M. J. Blaser, and M. Romano. 1996. Effect of *Helicobacter pylori* on gastric epithelial cell migration and proliferation *in vitro*: role of VacA and CagA. *Infect. Immun.* 64: 2829–2833.
53. Dunn, A. K., D. S. Millikan, D. M. Adin, J. L. Bose, and E. V. Stabb. 2006. New rfp- and pES213-derived tools for analyzing symbiotic *Vibrio fischeri* reveal patterns of infection and lux expression in situ. *Appl. Environ. Microbiol.* 72: 802–810.